Stable Charged-Particle Acceleration and Focusing in a Laser Accelerator Using Spatial Harmonics

B. Naranjo, A. Valloni, S. Putterman, and J. B. Rosenzweig

Department of Physics and Astronomy, University of California, Los Angeles, California 90095-1547, USA

(Received 13 October 2011; revised manuscript received 25 June 2012; published 19 October 2012)

Regarding the laser-driven acceleration of charged particles in photonic systems, a central unmet challenge is the achievement of simultaneous transverse and longitudinal stability at nonultrarelativistic energies. At such energies, Earnshaw's theorem [S. Earnshaw, Trans. Cambridge Philos. Soc. **7**, 97 (1842)] indicates that a synchronous accelerating wave gives a defocusing effect. We present a scheme in which particles are accelerated by interaction with a resonant spatial harmonic and are focused by strong ponderomotive interaction with nonresonant spatial harmonics. We show that this scheme exhibits net transverse focusing and longitudinal stability, and we discuss its use in a compact laser accelerator.

DOI: 10.1103/PhysRevLett.109.164803 PACS numbers: 41.75.Jv, 29.27.−a, 41.75.Lx

To meet the needs of future high-energy physics accelerators and x-ray free-electron lasers, there has been significant recent research into very high field ($>\mathrm{GV/m}$) acceleration techniques [1,2] that hybridize existing accelerator technology with optical technology such as lasers [3,4] and photonic band-gap crystals [5]. To permit operation at very high fields in the optical regime, a laser structure accelerator (LSA) should abandon the use of metals in favor of dielectrics [6]. In contrast to the near-axisymmetry used in standard radio frequency (rf) linear accelerators (linacs), the system should have a field configuration with approximately two-dimensional Cartesian symmetry [4,5]. This transverse asymmetry gives two advantages that permit large charge fluxes. First, space-charge self-forces, which are highly disruptive at low energy, are geometrically mitigated. Second, destabilizing transverse wakefields, which are a significant challenge in high-frequency accelerators, are greatly diminished [7].

The charged-particle dynamics in LSAs present distinct challenges. In an accelerating wave of magnitude E and wave vector k, a charged particle's longitudinal dynamics may be categorized according to the ratio of its increase in γ to its advance in phase, $\alpha = qE/kmc^2$. Electron dynamics in rf linacs, where $\alpha \sim 1$, are straightforward in that the electrons' phase motion quickly becomes negligible, as relativistic velocities are achieved early in the acceleration process. In contrast, for $\alpha \ll 1$, appropriate for ions in rf linacs and electrons in GV/m infrared LSAs, the dynamics are more intricate and are described in terms of stable regions, termed "buckets," localized in longitudinal phase space around resonant nonultrarelativistic velocities. For electron LSAs, the time scale of this motion is sub-fs and the beam's narrow transverse dimension is on the scale of microns. Accordingly, an LSA should employ very small normalized emittances, $\epsilon_{y,n} \simeq 10^{-9}$–$10^{-10}$ m · rad, as well as an effective focusing scheme. In proton linacs, synchronous defocusing is counteracted by use of external focusing. This approach may not be used in optical accelerators, as the length scales are too short for standard magnetic devices. Thus, one is forced to examine focusing provided by the second-order transverse forces associated with the electromagnetic mode itself. Second-order focal effects are obtained by varying the fields in a time-dependent fashion, for which Xie has proposed an alternating phase scheme [8]. However, the resultant second-order acceleration is quite complex and inherently weak.

Addressing these dynamics problems, we propose a new scheme that utilizes an accelerator eigenmode consisting of multiple spatial harmonics. Acceleration is provided by a resonant spatial harmonic, while second-order focusing [9] sufficient to overcome the resonant wave's defocusing is provided by nonresonant spatial harmonics. Furthermore, we demonstrate that the longitudinal motion associated with the resonant bucket is not destabilized by the presence of these perturbing nonresonant waves.

Consider a dielectric periodic along the beam axis, $\epsilon(\mathbf{x}_\perp, z) = \epsilon(\mathbf{x}_\perp, z + d)$. The electric field of a mode having wave vector $k\hat{\mathbf{z}}$ and angular frequency ω can then be written in Floquet form, $\mathbf{E}(\mathbf{x}, t) = E_0 e^{i(kz-\omega t)}\mathbf{u}(\mathbf{x})$, where $\mathbf{u}(\mathbf{x}_\perp, z + d) = \mathbf{u}(\mathbf{x}_\perp, z)$. Assuming the convention that k lies in the first Brillouin zone, $-\pi/d < k \leq \pi/d$. Because $\mathbf{u}$ is periodic in z, one may write the longitudinal field as

$$E_z = -iE_0 \sum_{n_z} a_{n_z} e^{i(k_{n_z} z-\omega t)}, \tag{1}$$

where $k_{n_z} = k + 2\pi n_z/d$, and the sum is taken over all integers n_z. For later convenience, an overall phase of $-i$ has been extracted. The field in Eq. (1) is decomposed into spatial harmonics, each having the same temporal frequency but different phase velocity $v_{n_z} = \omega/k_{n_z}$. Acceleration by resonant interaction occurs when the particle's velocity is nearly equal to the phase velocity of one of the spatial harmonics, which we label n_0.

As the essential features are present in a simplified 2D analysis, all field variation with x is dropped for now.

 © 2012 American Physical Society

Therefore, one may classify the modes as to whether the field in the plane is electric or magnetic [10]. To permit acceleration along the z axis, assume that the mode under consideration is electric in the plane, so that the only nonvanishing field components are E_y, E_z, and B_x. Further assume that the dielectric has mirror symmetry about the $y = 0$ plane, $\epsilon(\mathbf{x}) = \epsilon(\mathcal{M}_y\mathbf{x})$, where the mirror-reflection operator $\mathcal{M}_y$ is defined by its action on a three-vector, $\mathcal{M}_y\langle v_x, v_y, v_z\rangle = \langle v_x, -v_y, v_z\rangle$. Combining this with our previous assumption that $\mathbf{k}$ lies along the z axis, the fields are either even (upper sign) or odd (lower sign) under y reflection [10],

$$\mathcal{M}_y\mathbf{E}(\mathcal{M}_y\mathbf{x}) = \pm\mathbf{E}(\mathbf{x}) \quad \text{and} \quad \mathcal{M}_y\mathbf{B}(\mathcal{M}_y\mathbf{x}) = \mp\mathbf{B}(\mathbf{x}).$$

Consistent with the demands of focusing and acceleration, only consider even modes so that E_y and B_x are odd functions about $y = 0$, while E_z is an even function about $y = 0$. For small displacements y from the beam axis $(y/d \ll 1)$ to lowest nonvanishing order, Gauss's law, $E_y \simeq -y(\partial E_z/\partial z)$, gives

$$E_y \simeq -yE_0\sum_{n_z} a_{n_z}k_{n_z}e^{i(k_{n_z}z-\omega t)}.$$

Likewise, the lowest order transverse component of the magnetic field from Ampère's law, $B_x \simeq -(y/c^2)(\partial E_z/\partial t)$, is obtained giving

$$B_x \simeq \frac{yE_0}{c^2}\sum_{n_z} a_{n_z}k_{n_z}v_{n_z}e^{i(k_{n_z}z-\omega t)}.$$

One final simplifying assumption is that all of the amplitudes a_{n_z} are real, which can always be arranged for a dielectric lattice having both spatial-inversion and time-reversal symmetries. Without loss of generality, set $a_{n_0} = 1$.

For an electron traveling at approximately the resonant phase velocity, we substitute $\zeta = z - v_{n_0}t$ and define $\omega_{n_0} \equiv 2\pi\omega/k_{n_0}d$ so that the Lorentz force $\mathbf{F} = -e(\mathbf{E} + v_{n_0}\hat{\mathbf{z}}\times\mathbf{B})$ may be written

$$F_i(\mathbf{x}, t) = \mathrm{Re}\sum_q f_{i,q}(\mathbf{x})e^{iq\omega_{n_0}t}, \tag{2}$$

where the sum is over all integers q and

$$f_{y,q} = yeE_0a_{n_0+q}k_{n_0+q}(1 - \beta_{n_0}\beta_{n_0+q})e^{ik_{n_0+q}\zeta},$$
$$f_{z,q} = ieE_0a_{n_0+q}e^{ik_{n_0+q}\zeta}.$$

Several observations are made of the Lorentz force. First, the resonant spatial harmonic $q = 0$ is considered. Defining the particle phase $\phi \equiv k_{n_0}\zeta$, the transverse and longitudinal contributions are $(yeE_0k_{n_0}/\gamma_{n_0}^2)\cos\phi$ and $-eE_0\sin\phi$, respectively. For stable longitudinal acceleration, which requires $-\pi/2 < \phi < 0$, the transverse force is defocusing. Second, the nonresonant spatial harmonics $q \neq 0$ is considered. The transverse components vanish for $v_{n_0}v_{n_0+q} = c^2$ and are otherwise proportional to $k_{n_0+q} - \beta_{n_0}^2k_{n_0}$.

Following the analysis of Ref. [11], the electron motion is separated into a slowly varying "secular" component $X_i(t)$ and a rapidly varying component $\xi_i(t)$, $x_i(t) = X_i(t) + \xi_i(t)$, so that the secular equations of motion for a force having the form of Eq. (2) are

$$m_e\gamma_{n_0}^{1+2\delta_{i,z}}\ddot{X}_i = \mathrm{Re}[f_{i,0}(\mathbf{X})] - \sum_j\sum_{q\neq 0}\frac{1}{2m_e\gamma_{n_0}^{1+2\delta_{j,z}}q^2\omega_{n_0}^2} \times \mathrm{Re}\left[\frac{\partial f_{i,q}}{\partial x_j}(f_{j,q}^* + f_{j,-q})\right]_{\mathbf{X}}.$$

Adopting the beam physics convention of using z as the independent variable and introducing the notation $()' \equiv d/dz = (1/v_{n_0})d/dt$,

$$Y'' = Y\left\{\frac{\alpha_{n_0}k_{n_0}^2}{\gamma_{n_0}^3\beta_{n_0}^2}\cos\phi - \frac{\alpha_{n_0}^2\omega^2}{2\gamma_{n_0}^2\beta_{n_0}^4\omega_{n_0}^2}[(B + D) + (C + E)\cos 2\phi]\right\}, \tag{3}$$

where

$$\alpha_{n_0} \equiv \frac{eE_0}{k_{n_0}m_ec^2} = \frac{eE_0\beta_{n_0}\lambda}{2\pi m_ec^2}(e > 0),$$
$$B = \sum_{q\neq 0}\frac{a_{n_0+q}^2k_{n_0+q}^2}{q^2}(1 - \beta_{n_0}\beta_{n_0+q})^2,$$
$$C = \sum_{q\neq 0}\frac{a_{n_0+q}a_{n_0-q}k_{n_0+q}k_{n_0-q}}{q^2} \times (1 - \beta_{n_0}\beta_{n_0+q})(1 - \beta_{n_0}\beta_{n_0-q}),$$
$$D = \frac{1}{\gamma_{n_0}^2}\sum_{q\neq 0}\frac{a_{n_0+q}^2k_{n_0+q}^2(1 - \beta_{n_0}\beta_{n_0+q})}{q^2},$$
$$E = -\frac{1}{\gamma_{n_0}^2}\sum_{q\neq 0}\frac{a_{n_0+q}a_{n_0-q}k_{n_0+q}^2(1 - \beta_{n_0}\beta_{n_0+q})}{q^2}.$$

The transverse secular equation of motion, Eq. (3), yields the criteria for simultaneous acceleration and stabilization. The term linear in E_0 is the resonant defocusing term, and the term quadratic in E_0 is the average effect of the rapidly oscillating nonresonant spatial harmonics. More specifically, the terms B and C are due to the rapid transverse motion, whereas the terms D and E are due to the rapid longitudinal motion. The direct terms B and D are unconditionally focusing, whereas the interference terms C and E are either focusing or defocusing, depending on the particle phase ϕ. These interference terms result from a nonresonant spatial harmonic driving the rapid motion, while an oppositely traveling wave, relative to the synchronous frame, is sampled by the averaging procedure.

Because the ponderomotive focusing terms in Eq. (3) are proportional to $1/q^2\omega_{n_0}^2$, the focusing strength can be significantly increased by reducing $\omega_{n_0} = 2\pi v_{n_0}/d$. Consider, at first, a photonic accelerator whose longitudinal periodicity

d is of the same order as the photonic lattice constant a. As useful photonic band gaps typically lie in the frequency range $\omega a/2\pi c = a/\lambda \sim 1$, one has $\omega_{n_0} \sim \beta_{n_0}\omega$. Therefore, the frequencies of the rapidly varying forces are in the optical range, and the ponderomotive focusing force remains correspondingly weak. If, instead, we consider a photonic accelerator whose smallest repeating length (i.e., the primitive lattice constant) along the longitudinal direction is $d = \mathrm{Na}$, then $\omega_{n_0} \sim \beta_{n_0}\omega/N$ and the ponderomotive focusing force grows correspondingly strong. We specify that d is then primitive so that both of the $q = \pm 1$ spatial harmonics do not identically vanish by symmetry.

Breakdown ultimately limits the peak axial field that can be used. For the accelerator eigenmodes under consideration, the peak axial field is typically larger than the peak dielectric field, roughly $E_{\text{peak axial}}/E_{\text{peak dielect}} \sim 1.5$. The breakdown electric field for a pulse propagating in a dielectric [12] is $E_{\text{peak dielect}} = \sqrt{F_{\text{th}}/\tau c\epsilon_0}$, where F_{th} is the material's damage threshold and τ is the pulse length. Due to its high dielectric coefficient and compatibility with microfabrication techniques, we are strongly considering silicon at 5 μm. The damage threshold has yet to be measured in silicon at 5 μm for $\lesssim$ ps pulses, but Soong *et al.* [13] measured $F_{\text{th}} = 0.35\ \text{J/cm}^2$ at 2.2 μm for 1 ps pulses. At 5 μm, multiphoton ionization will be weaker, but tunnel ionization will be stronger. Using this value of F_{th} and $\tau = 80$ fs gives $E_{\text{peak axial}} = 6\ \text{GV/m}$. Other promising materials in the infrared are sapphire and quartz, which have more than an order-of-magnitude improvement in F_{th} over silicon, at the cost of a smaller dielectric constant.

Consider the case where the only nonvanishing nonresonant spatial harmonic is $q = +1$, which provides two simplifications. First, it avoids interference terms in the transverse secular equation of motion, so that $C = E = 0$ in Eq. (3). Second, taking the nonresonant spatial harmonic to be slower ($q > 0$) than the resonant spatial harmonics avoids the mutual cancellation of the transverse electric and magnetic forces at $v_{n_0}v_{n_0+q} = c^2$. Comparing the resonant defocusing force's maximum value at $\phi = 0$ with the nonresonant focusing force's minimum value (in this case, the focusing force does not depend on ϕ) yields the transverse stability diagram shown in Fig. 1.

Having identified the transverse stability condition, we now concentrate on longitudinal dynamics. Examining briefly only the effect of the resonant wave, we define the momentum deviation $\delta p \equiv p_z - p_{n_0}$, where $p_{n_0} = \gamma_{n_0}\beta_{n_0}m_e c$. Then, we write the electron's small-amplitude longitudinal Hamiltonian as [14]

$$H(\zeta, \delta p) \approx (m_e c^2)\left[\frac{\beta_{n_0}^2(\delta p)^2}{2\gamma_{n_0}p_{n_0}^2} - \alpha_{n_0}(\cos\phi + \phi\sin\phi_0)\right],$$

where we have allowed for an accelerating bucket by setting the synchronous phase $\phi_0 < 0$. As this

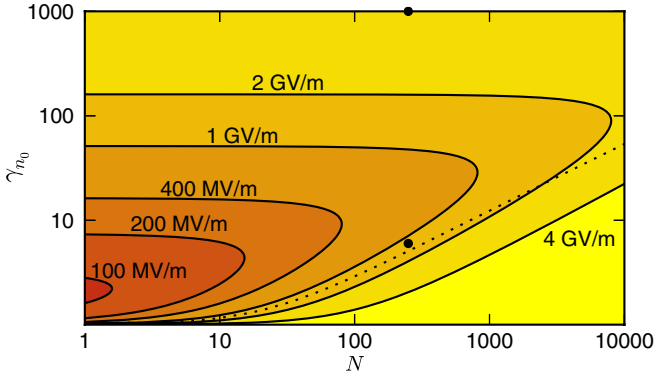

FIG. 1 (color online). Stability diagram for a single nonresonant spatial harmonic $a_{n_0+1} \neq 0$. Increasing the slow modulation length N and increasing the particle energy γ_{n_0} improves transverse stability and gives higher values of the accelerating field E_0 for a fixed net field $E_0(1 + |a_{n_0+1}|) = 6$ GV/m. Locations of the two example cases discussed in the text are shown with dot markers. The region below the dotted line ($\eta = 0.03$) is longitudinally unstable. ($a = 1.15$ μm and $\lambda = 5$ μm).

Hamiltonian is a constant of the motion, one may deduce the dimensions of the stable bucket in longitudinal phase space.

To examine the dynamics in the presence of nonresonant harmonics, the equation of motion is numerically solved as

$$\frac{d(\delta p/p_{n_0})}{d\tilde{t}} = \frac{-\alpha_{n_0}k_{n_0}d}{\beta_{n_0}^2\gamma_{n_0}}\Big[(\sin\phi - \sin\phi_0) + \sum_{q\neq 0} a_{n_0+q}\sin[(k_{n_0+q}/k_{n_0})\phi + 2\pi q\tilde{t}]\Big]$$
$$\frac{d\phi}{d\tilde{t}} = \frac{k_{n_0}d}{\gamma_{n_0}^2}(\delta p/p_{n_0}), \tag{4}$$

where $\tilde{t} \equiv \omega_{n_0}t/(2\pi)$ is a dimensionless time variable normalized so that $\Delta\tilde{t} = 1$ corresponds to a single period of the micromotion's lowest frequency components ($q = \pm 1$).

Two example cases, $\gamma_{n_0} = 6$ and $\gamma_{n_0} = 1000$, with stable acceleration parameters, are shown in Table I. Simultaneously integrating both the longitudinal equation of motion, Eq. (4), and the transverse equation of motion, $m_e\gamma\ddot{y} = F_y$, both of these cases were verified to be stable. Figure 2 shows longitudinal phase-space trajectories for the $\gamma_{n_0} = 6$ case. Even with such large amplitude perturbing waves, a stable bucket structure is observed. Though

TABLE I. Low- and high-energy example cases yielding transverse and longitudinal stability with accelerating gradients ≥ 1 GeV/m. [$N = 250$ and $E_0(1 + a_{n_0+1}) = 6$ GV/m].

γ_{n_0}	E_0 (GV/m)	$a_{n_0+1}E_0$ (GV/m)	GeV/m
6	1.414	4.586	1.0
1000	3.536	2.464	2.5

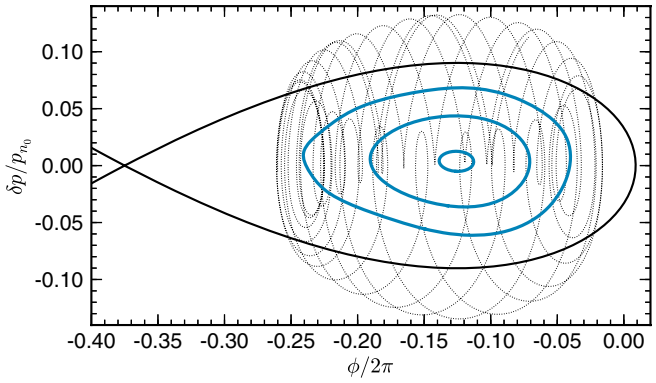

FIG. 2 (color online). Longitudinal phase-space trajectories for a bucket having acceleration gradient 1 GeV/m being perturbed by a strong nonresonant wave. The blue orbits are obtained by averaging the phase space motion over a single period $\Delta\tilde{t} = 1$. The dotted line is the raw phase-space motion for the outermost blue orbit, showing the rather violent nonresonant longitudinal motion that provides approximately 40% of the transverse stability in this case. The black line is the separatrix obtained from the unperturbed Hamiltonian. [$N = 250$, $\gamma_{n_0} = 6$, $E_{n_0} = \sqrt{2}$ GV/m, $E_0(1 + a_{n_0+1}) = 6$ GV/m, $\phi_0 = -\pi/4$].

increasing N improves transverse stability, it also moves the nonresonant buckets closer to the resonant buckets. When the border regions of the two buckets overlap, the trajectories become longitudinally unstable according to the Chirikov criterion [15]. For instance, in Fig. 2, the nonresonant buckets travel towards the left and are located at $\delta p/p_{n_0} = -0.33$, far enough below the resonant buckets to not destabilize the trajectories. An approximately equivalent longitudinal stability criterion,

$$\Delta\left(\frac{\phi_q}{2\pi}\right) = \frac{k_{n_0} e E_0 a_{n_0+q}}{2\pi m \gamma_{n_0}^3 q^2 \omega_{n_0}^2} = \eta,$$

is shown in Fig. 1, where η has been determined via comparison with numerical results.

We now give a brief example of a band-gap-confined waveguide accelerator that provides nonresonant focusing. It consists of a linear channel and a triangular lattice of holes etched into silicon (see Fig. 3 and movies in Supplemental Material [16]). The channel width is modulated over a distance of $d = 8a$, where a is the lattice constant. This provides a mix of spatial harmonics, particularly a slow sideband and a fast sideband. The beam is synchronized to the fast sideband, labeled $q = 0$ in Fig. 4(a). Then the $q = 1$ spatial harmonic provides the majority of nonresonant focusing, as shown by the spatial harmonic spectrum in Fig. 4(b). To design for large N, we treat the slow modulation as a cyclic adiabatic variation [17]. This 2D design can be generalized to a 3D design incorporating either a single finite slab or a stack of finite slabs. In 3D, the mode is confined in the plane by total internal reflection, provided that the spatial

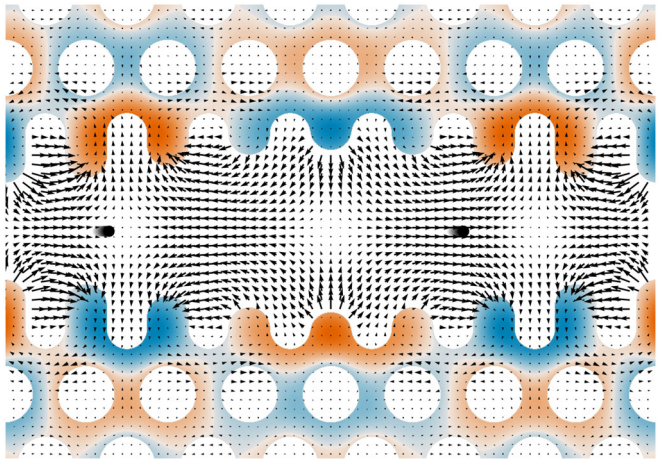

FIG. 3 (color online). Accelerator eigenmode simultaneously providing both transverse focusing and longitudinal acceleration. Arrows indicate electric field, and color shading indicates magnetic field in silicon. Unshaded channel in center and holes represent vacuum. Slow modulation of the waveguide fingers ($N = 8$) produces two sidebands about the unmodulated waveguide mode. Beam is synchronized to the fast sideband. Here, we take the design particles to be positrons, so that the synchronous phase ϕ_0 is $3\pi/4$. See movies in Supplemental Material [16]. ($a = 1.15$ μm and $\lambda = 5$ μm)

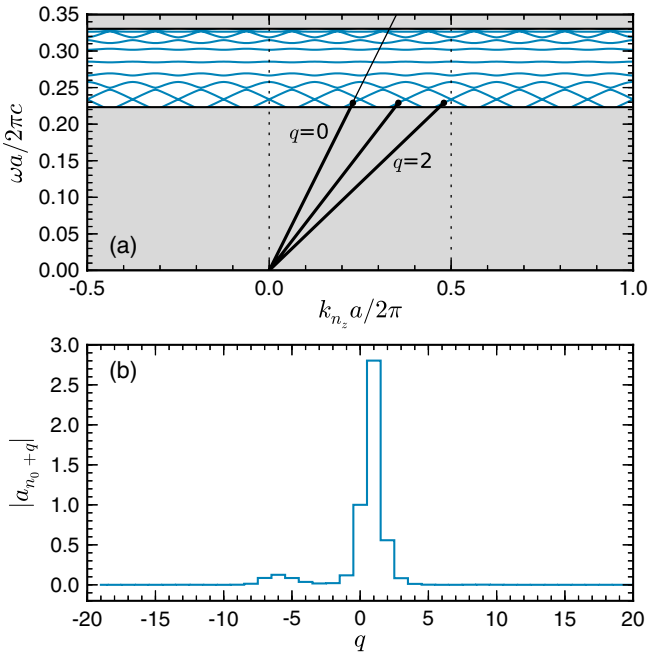

FIG. 4 (color online). Spectral properties of the accelerator eigenmode shown in Fig. 3. (a) Band diagram. Three spatial harmonics are shown with thick lines. The fast sideband, $q = 0$, is the resonant spatial harmonic and is approximately speed-of-light. The strongest nonresonant harmonic, $q = 1$, is slightly slower and provides the majority of the transverse focusing. (b) Spatial harmonic spectrum. The strength of the two sidebands, $q = 0$ and $q = 2$, relative to the unmodulated spatial harmonic, $q = 1$, can be increased by increasing the depth of the slow modulation.

harmonics are mostly underneath the light cone. For transverse particle confinement in the x direction, the mode can be adjusted so that it is resonantly focusing.

The approach presented here thus provides simultaneous transverse and longitudinal stability, as shown by relevant examples. The application of these results now takes on a certain urgency, as it may be essential in guiding LSA structure designs in numerous research programs, including an all-optical free-electron laser, with both accelerator and undulator [18] driven by lasers.

This work is supported by DARPA under Contract No. N66001-11-1-4197, the U.S. DOE under Contracts No. DE-FG02-07ER46272 and No. DE-FG03-92ER40693, and the ONR under Contract No. N00014-06-1-0925. B. N. and S. P. wish to thank DARPA MTO for support under the SERS program, covering work on photonic accelerators.

[1] I. Blumenfeld, C. E. Clayton, F.-J. Decker, M. J. Hogan, C. Huang, R. Ischebeck, R. Iverson, C. Joshi, T. Katsouleas, N. Kirby *et al.*, Nature (London) **445**, 741 (2007).

[2] W. P. Leemans, B. Nagler, A. J. Gonsalves, C. Toth, K. Nakamura, C. G. R. Geddes, E. Esarey, C. B. Schroeder, and S. M. Hooker, Nat. Phys. **2**, 696 (2006).

[3] X. E. Lin, Phys. Rev. ST Accel. Beams **4**, 051301 (2001).

[4] Z. Zhang, S. G. Tantawi, and R. D. Ruth, Phys. Rev. ST Accel. Beams **8**, 071302 (2005).

[5] B. M. Cowan, Phys. Rev. ST Accel. Beams **11**, 011301 (2008).

[6] J. Rosenzweig, A. Murokh, and C. Pellegrini, Phys. Rev. Lett. **74**, 2467 (1995).

[7] A. Tremaine, J. Rosenzweig, and P. Schoessow, Phys. Rev. E **56**, 7204 (1997).

[8] M. Xie, in *Proceedings of the European Particle Accelerator Conference* (JACOW, Vienna, 2000), p. 895.

[9] J. Rosenzweig and L. Serafini, Phys. Rev. E **49**, 1599 (1994).

[10] J. D. Joannopoulos, S. G. Johnson, J. N. Winn, and R. D. Meade, *Photonic Crystals: Molding the Flow of Light* (Princeton University Press, Princeton, NJ, 2008), 2nd ed.

[11] L. D. Landau and E. M. Lifshitz, *Mechanics*, Course of Theoretical Physics Vol. 1 (Pergamon Press, Oxford, 1976), 3rd ed.

[12] C. McGuinness, E. Colby, and R. L. Byer, J. Mod. Opt. **56**, 2142 (2009).

[13] K. Soong, R. L. Byer, C. McGuinness, and E. Peralta, in *Proc. of 2011 Particle Accelerator Conf.* (IEEE, New York, 2011), p. 277.

[14] J. Rosenzweig, *Fundamentals of Beam Physics* (Oxford University Press, New York, 2003).

[15] B. V. Chirikov, J. Nucl. Energy, Part C **1**, 253 (1960).

[16] See Supplemental Material at http://link.aps.org/supplemental/10.1103/PhysRevLett.109.164803 for movies of accelerator eigenmode.

[17] S. G. Johnson, P. Bienstman, M. A. Skorobogatiy, M. Ibanescu, E. Lidorikis, and J. D. Joannopoulos, Phys. Rev. E **66**, 066608 (2002).

[18] T. Plettner and R. L. Byer, Phys. Rev. ST Accel. Beams **11**, 030704 (2008).